

A lone spike in blood glucose can enhance the thrombo-inflammatory response in cortical venules

Journal of Cerebral Blood Flow & Metabolism
0(0) 1–20
© The Author(s) 2023
Article reuse guidelines:
sagepub.com/journals-permissions
DOI: 10.1177/0271678X231203023
journals.sagepub.com/home/jcbfm



Iftach Shaked^{1,2}, Conrad Foo^{1,*}, Philipp Mächler^{1,*}, Rui Liu¹, Yingying Cui¹, Xiang Ji¹, Thomas Broggini¹, Tomasz Kaminski³, Suchita Suryakant Jadhav², Prithu Sundd³, Michael Firer², Anna Devor⁴, Beth Friedman⁵ and David Kleinfeld^{1,6}

Abstract

How transient hyperglycemia contributes to cerebro-vascular disease has been a challenge to study under controlled physiological conditions. We use amplified, ultrashort laser-pulses to physically disrupt brain-venule endothelium at targeted locations. This vessel disruption is performed in conjunction with transient hyperglycemia from a single injection of metabolically active *D*-glucose into healthy mice. The observed real-time responses to laser-induced disruption include rapid serum extravasation, platelet aggregation, and neutrophil recruitment. Thrombo-inflammation is pharmacologically ameliorated by a platelet inhibitor, by a scavenger of reactive oxygen species, and by a nitric oxide donor. As a control, vessel thrombo-inflammation is significantly reduced in mice injected with metabolically inert *L*-glucose. Venules in mice with diabetes show a similar response to laser-induced disruption and damage is reduced by restoration of normo-glycemia. Our approach provides a controlled method to probe synergies between transient metabolic and physical vascular perturbations and can reveal new aspects of brain pathophysiology.

Keywords

Imaging, neutrophils, platelets, reactive oxygen species, transient hyperglycemia

Received 8 October 2022; Revised 14 August 2023; Accepted 21 August 2023

Introduction

Transient hyperglycemia secondary to metabolic demands and various stressors has been linked to adverse ischemic stroke outcomes^{1–3} and long-lasting effects on the patency of vessels.⁴ Transient hyperglycemia is not uncommon as shown⁵ from glucose monitoring in humans where high glucose transient spikes can reach prediabetic and even diabetic levels. These spikes in blood glucose concentration are variously attributed to rapid, high caloric intake, endocrine imbalances, and stressors including inflammation⁶ and chronic social stress.⁷

Numerous results in model systems suggest a link between high glucose and a prothrombotic phenotype.⁸ The formation of platelet-rich thrombi is initiated, at least in part, by soluble vascular stress signals such as thrombin, epinephrine, and adenosine diphosphate,⁹ as well as by exposure to collagen and laminin components of the extracellular matrix of a disrupted vessel.¹⁰

¹Department of Physics, University of California at San Diego, La Jolla, CA, USA

²The Adelson Medical School, Ariel University, Ariel, Israel

³Vascular Medicine Institute, University of Pittsburgh, Pittsburgh, PA, USA

⁴Department of Biomedical Engineering, Boston University, Boston, MA, USA

⁵Department of Computer Science and Engineering, University of California at San Diego, La Jolla, CA, USA

⁶Department of Neurobiology, University of California at San Diego, La Jolla, CA, USA

*Equal contribution.

Corresponding authors:

Beth Friedman, Department of Computer Engineering, University of California San Diego, La Jolla, California, CA 92093-0021, USA.
Email: befriedman@ucsd.edu

David Kleinfeld, University of California at San Diego, La Jolla, California, CA 92093-0319, USA.
Email: dk@physics.ucsd.edu

It is suggested that hyperglycemia increases platelet responsiveness to such agonists.¹¹ Mechanistically, hyperglycemia increases production of mitochondrial reactive oxygen species (ROS) in primary endothelial cells *in vitro*¹² and the constellation of ROS mediated pathogenic pathways provides a basis for the endothelial dysfunction observed in people with diabetes.^{13–15} Importantly, blood fluidity is impacted by ROS through associated depletion of the vasoactive gaseous transmitter nitric oxide. This gas molecule is an essential cofactor for vasodilation¹⁶ and further functions as a checkpoint for inhibition of platelet activation.¹⁷ Platelet activation in turn initiates an inflammatory cascade that is mediated, in part, by neutrophil recruitment.¹⁸

To establish a potential link between a spike in blood glucose concentration in the blood stream and a prothrombotic phenotype *in vivo*, we introduce a new model of vascular tissue disruption. Our model uses amplified ultra-short laser pulses targeted to cerebral veins as a surrogate for injuries that lead to platelet activation. In their pioneering work, the Furies used laser induced vascular disruption as a means to track thrombus formation within the cremaster artery of anesthetized rats,¹⁹ to mimic the pathophysiology of spontaneous vessel wall tissue disruption that may be variously triggered by high wall-shear stress,²⁰ infection,²¹ and aging.²² Our experimental platform features the use of focused nonlinear optical excitation for vessel disruption. Since there is no thermal damage to the vessel wall^{23,24} we can precisely induce single vessel tissue disruption with minimal collateral damage. We further make use of transcranial imaging to minimize craniotomy-induced inflammation²⁵ and to preserve brain homeostasis²⁶ in awake mice. These advances extend prior use of focused nonlinear optical excitation to ablate individual blood vessels^{27,28} and somata^{29,30} *in vivo*.

We chose to target cortical cerebral venules for disruption as the central sinus and venous branches act as an immune hub, with both innate and adaptive immune activity³¹ that may contribute to cerebral venous thrombosis. Further, the tree-like topology of pial venules³² allows us to perform injuries of multiple independent venous segments in single mice with transient hyperglycemia. Finally, we are motivated to study CNS thrombotic events by data that suggests that thrombotic events are organ specific and peripheral vascular beds are non-identical to those of the CNS.^{33–35}

Materials and methods

Subjects

All animal procedures were approved by the Institutional Animal Care and Use Committee

(IACUC) at the University of California, San Diego (UCSD) and follow or exceed those described in the United States National Institutes of Health “Guide for the Care and Use of Laboratory Animals”, Publication 85–23 (1985). Our subjects were C57BL/6J wild type, LysM-eGFP, db/db, and STZ treated mice, all males between age P55 and P75, and all from The Jackson Laboratory.

Transient hyperglycemia. To transiently modulate blood sugar, *L*-glucose (*L*-glc) or *D*-glucose (*D*-glc) (Sigma) solutions were *i.p.* injected at 2 gm/kg mouse body weight, 20% (w/v) in saline, following 18 hours fast, 30 minutes prior to the laser induced vascular disruption. Blood sugar levels were monitored (3–5 μ l samples) from the tail vein with a glucometer (Contour[®]).

Chronic hyperglycemia. We used streptozotocin (STZ) induced type 1 diabetes mice. Streptozotocin induced mice display chronic hypoinsulinemia and hyperglycemia. This form of chronic hyperglycemia can be transiently reversed by a single *i.p.* injection of insulin (1 unit/kg (TOCRIS-#3435)). As a model of type 2 diabetes mellitus, we used leptin receptor deficient *db/db* mice, which display obesity and insulin resistance evidenced by severe hyperglycemia.

Intraperitoneal (IP) injections. Pharmacological modulators were administered by *i.p.* injection. The ADP receptor P2Y₁₂ blocker, Clopidogrel (1 mg/kg) (TOCRIS #2490), was administered one day before imaging. The NO donor S-nitroso-N-acetyl-DL-penicillamine (SNAP) (Sigma-Aldrich #N3398) (5 mg/kg), was administered one hour before the onset of imaging. The mitochondrial oxygen free radical scavenger, MitoTempo (10 mg/kg) (Sigma SML 0737), was administered one day before imaging with a second boost one hour before imaging.

Surgery. Eight-week-old mice were anesthetized with isoflurane, 3% (v/v) oxygen for induction and 1.5%–2.5% (v/v) for maintenance, from a precision vaporizer. Reflexes and breathing were visually monitored through the entire surgical procedure to ensure a deep plane of anesthesia. Body temperature was maintained at 37 °C using a heating pad with feedback regulation (FHC, model 40-90-8 D). The animal was then placed in a stereotaxic frame, and the periosteum on the parietal and occipital plates was exposed, only skull sutures were covered with low viscosity cyanoacrylate glue (Loctite, no. 4104) to reinforce stability between skull plates, and a 1.5 mm by 1.5 mm region of skull over somatosensory cortex was thinned with a 250 μ m drill bur coupled to a low vibration drill (Osada, EXL-M40) to form a transcranial window.^{26,36} The thinned bone was dried and covered with cyanoacrylate glue

(Loctite, no. 401) and a number 0 glass coverslip and a T-shaped metal implant was glued onto the skull for head-fixation. The remaining exposed bone and the implant were covered with cyanoacrylate glue and dental cement (Grip Cement, Denstply no. 675571) to increase stability. Buprenorphine hydrochloride (Buprenex, Reckitt Benckiser Pharmaceuticals) was provided subcutaneously for analgesia (7 μ g) as the animal recovered from surgery. Mice were allowed to recover for 48–72 hours before experiments were performed.

Retro-orbital injection. Labeling of blood serum was achieved with Texas red dextran (2 MDa) (ThermoFisher T6134), Alexa Fluor 405 (AF405) dextran (2 MDa), or fluorescein isothiocyanate–dextran (2 MDa) (FITC–dextran; Sigma-Aldrich FD2000S). Labelling of platelets was achieved using Biotin anti-mouse CD41 (integrin alpha 2 b) antibody (BioLegend #133930) conjugated with Streptavidin Alexa Fluor™ 594 or Streptavidin 405 (ThermoFisher Scientific #S11227, #S32351).

In vivo imaging and laser induction of intravascular blood platelet aggregates

Live images of mouse cerebral vasculature were obtained with a system of local design in which a two-photon laser scanning microscope incorporates a beam line from an amplified 100-femtosecond pulsed laser.³⁷ The utility of this design is described in detail in prior work,^{27,38,39} we extend the system to produce micrometer-sized regions of damage to the lumen of a vessel in the intact skull. See Supplemental Material for details. Selected acquisition of precision in vivo images used an adaptive optics configuration of two-photon imaging.⁴⁰

Acquisition. Individual frames were acquired at 2.13 Hz using standard galvanometric scanners (Figure 1(c)). The typical power levels used for imaging were within the range of 20 to 40 mWatts, at the brain surface, at a wavelength of 840 nm. We detected fluorescence with one of two schemes. For labeling of blood serum and platelets, we imaged Alexa Fluor™ 405 to monitor blood flow and serum extravasation (emission filtered at 457 ± 25 nm) and imaged Alexa Fluor™ 594 to monitor platelets (emission filtered at 615 ± 20 nm). For labeling of blood serum, platelets, and neutrophils, we imaged Alexa Fluor™ 405 to monitor platelets (emission filtered at 457 ± 25 nm), Texas Red to monitor blood flow and serum extravasation (emission filtered at 615 ± 20 nm), and EGFP to monitor neutrophils (emission filtered at 512 ± 12 nm).

We imaged single frames at the focal plane of the laser-induced damage for the first 412 s after laser-induced

vascular disruption and then performed a volumetric reconstruction between 413 and 882 s after the laser-induced vascular disruption. The scan was arranged to cross the focal plane of the platelet aggregates at a time of about 650 s after laser-induced damage. The volume consisted of 1000 scans; an axial z-stack in steps of 1 μ m across 100 μ m with an average of 10 frames per step. Oversampling and averaging was performed solely to improve the signal-to-noise ratio.

Blinded test

To test the effect of transient hyperglycemia in an unbiased manner we used randomized, blinded i.p. injection of *L*- or *D*-glc. Prior to each imaging session mice were fasted overnight (18 hr), then injected with *L*-glc; 2 gm/kg mouse body weight, 20% (w/v) in saline. Mice injected with *L*-glc were then imaged and platelet aggregate formation was induced and monitored. An identical second imaging/laser-induced damage session was then conducted with the same mouse, injected with a second unmarked tube that contained either *L*- or *D*-glc; 2 gm/kg mouse body weight of 20% (w/v) in saline. Importantly, each imaging session was carried out in a separate venule that branched from the central sinus.

Histology

Mice with transient hyperglycemia were euthanized by intravenous administration of pentobarbital at the end of in vivo imaging data collection (3 mice). The heads were removed, post-fixed en bloc and then decalcified in 0.5 M EDTA (Promega A2671) followed by sucrose cryoprotection. Serial cryo-stat sections were mounted on consecutive slides for application of different antibodies on adjacent sections.

Sections underwent antigen retrieval and immunostaining with antibodies that identify proteins that are up-regulated in activated endothelial cells. Von Willebrand factor antibody (Invitrogen, PA516634; 1:1000), was localized with biotinylated anti-rabbit antibody (Vector BA-1000) and Alexa 647-Streptavidin (1:200) (Life Technologies S32357). Anti-collagen IV antibody (Southern Biotech, 1340-1; 1:6000) was localized with biotinylated anti-goat antibody (Vector BA9500) and Alexa 647-Streptavidin. Intercellular Adhesion molecule-1 (ICAM-1; 1:2000) was localized from its conjugation to Alexa 647 (Abcam, ab307614). DAPI-Fluoromount-G (Southern Biotech 0100-20) cover-slipped slides were scanned for fluorescence with a Zeiss Axioscanner (325 nm/pixel) (FITC; ex 470 ± 20 nm, em 525 ± 25 nm) (Alexa 594; ex 590 ± 7 nm, em 624 ± 16 nm) (Alexa 647; ex 640 ± 15 nm; em 690 ± 25 nm) (DAPI; ex 385 ± 10 nm, em 425 ± 15 nm).

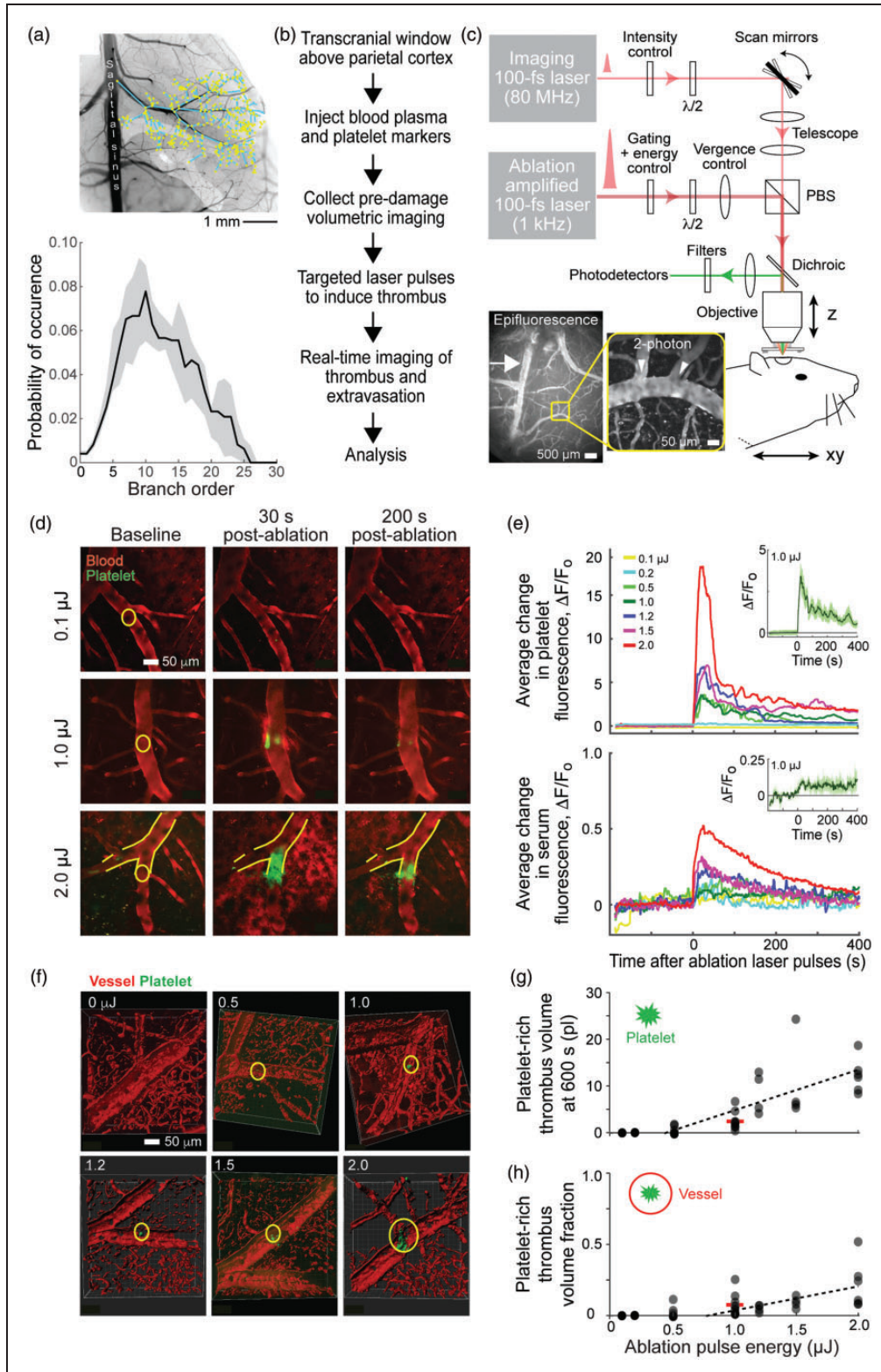


Figure 1. Sample preparation and calibration studies for cerebrovascular disruption by the targeted delivery of amplified ultra-short laser pulses. (a) Topology of the pial venules. The top diagram is taken from the reconstruction of vasculature in a single mouse. The bottom compilation incorporates 11 surface venules in five mice. (b) Timeline of study design. (c) Schematic representation of the optical system that combines two-photon laser scanning microscopy with optical ablation using a gated train of amplified ultra-short laser pulses. The inset is the image of surface vasculature of mouse cortex; arrow indicates branch of superior cerebral vein targeted for disruption. Continued.

Fibrinogen blood assay

Mice were fasted overnight. They were injected either with sterile saline or dosed with 2 g/kg of *D*-glc. Thirty minutes post saline or *D*-glc injection, 45 μ l of blood was collected from the tail vein supplemented with 5 μ l of sodium citrate (0.11 mol/L). Fibrinogen blood concentration was determined using a Healvet coagulation analyzer (HV-COA 7000).

Reactive oxygen species assay

Mice were randomly divided into two groups: *Vehicle* (injected with sterile saline) and *D*-glc (dosed at 2 g/kg). 30 minutes post vehicle/*D*-glc injection mice were anesthetized with an IP injection of a cocktail containing 100 mg/kg ketamine HCl (Covetrus) and 20 mg/kg xylazine (Akorn Pharmaceuticals). The blood (300 μ l) was collected using sodium citrate as an anticoagulant. Blood was centrifuged at 100 *g* for 10 minutes to obtain platelet-rich plasma (PRP, >98% of platelets) and the PRP was washed twice (1100 *g* for 15 minutes) using Hanks balanced salt solution without Ca^{2+} and Mg^{2+} (HBSS) (GIBCO 14175095) with the addition of 5 μ M prostaglandin I₂ as a potent inhibitor of platelet activation.

MitoSOX Red mitochondrial superoxide indicator (Invitrogen) was dissolved in DMSO (Sigma Aldrich) at a concentration of 1 mM, diluted to a 5 μ M working solution in pre-warmed HBSS prior to staining isolated the PRP and incubated at 37 °C for 30 min in the dark. The PRP was washed twice with warm HBSS to remove unbound dye and re-suspended in 200 μ l of warm HBSS. Flow cytometry measurements were carried out using a BD LSRFortessa (BD Biosciences). A laser at 488 nm excited MitoSOX and emission was collected at 575 ± 13 nm. Data is presented as the fraction of positive cells based on a histogram chart.

Quantification and statistical analysis

The reporting of our data is in compliance with the ARRIVE guidelines.⁴¹

All time-series analysis was done using MATLAB (MathWorks). Regions of interest (ROIs) were drawn around the laser damage site and the average pixel intensities of the ROI in multiple fluorescence channels were used to construct time series of platelet aggregation, neutrophil aggregation, and serum extravasation. Time series were normalized to the average of the 141 s of data acquired prior to the laser-induced vascular disruption, i.e., these data define F_0 at each pixel. We then calculated $\Delta F/F_0 = F(t)/F_0 - 1$. Time series were smoothed with 2.4 s median filter. Volumetric analysis was done on image stacks using Imaris (Oxford Instruments).

To determine the laser power needed to induce thrombosis, a piecewise linear model was fit to the platelet aggregates volume and platelet aggregates fraction as a function of laser energy using the Shape Language Modeling toolbox in MATLAB.⁴² The model had one free interior knot, i.e., the threshold power, and was constrained to be a constant value between 0 and 0.2 μ J of the laser pulse energy.

The two-sided unpaired Wilcoxon rank sum test was used to compare platelet and neutrophil volumes and volume fractions at 650 s across different experimental conditions.

The one-sided unpaired Wilcoxon rank sum test was used to compare time series of changes in blood component different experimental conditions. For blood serum, we used the average fluorescence of the last 100 s of the relevant times series. For platelet and neutrophil aggregation, the average fluorescence of the first 100 s of the times series after laser damage was compared across different experimental conditions.

A one-way Kruskal Wallis H-test was used to perform a meta-analysis of whether platelet aggregates

Figure 1. Continued.

laser-induced disruption. (d) Fluorescent images of platelet (anti-CD41; green) and serum (Texas red dextran) fluorescence in cortical surface veins, before and 30 s and 200 s post irradiation using 0.1 μ J, 1.0 μ J, and 2.0 μ J laser pulses. Focal region of the excitation spot is highlighted by the yellow circle. (e) Effects of varying laser energy, by increasing the power and keeping the number of pulses constant, on the time course of laser-induced aggregation of platelets and blood extravasation following the example data in panel D. Each curve is generated from the average change in vein fluorescence relative to baseline values (6 veins at one vein per animal at 0.1 μ J, 0.2 μ J, and 1.0 μ J; 3 for 1.2 μ J, and 1.5 μ J; 11 veins for 0.5 μ J; and 5 veins for 2.0 μ J); 40 mice total. Inset highlights the mean and standard error for the samples at 1.0 μ J. (f) Three-dimensional reconstructions of platelets aggregates (green) within vasculature (red), collected 400 to 600 s after laser-induced vascular disruption. (g) Platelet-rich thrombi volumes for data collected between 400 and 870 s after laser-induced vascular disruption; we mark the midpoint time of \sim 600 s post laser damage. Same veins as in panel E. The responses at 0.5 μ J is statistically different from zero ($p < 0.01$), as is the response at 1.0 μ J ($p < 0.01$). The red bar is the mean at 1.0 μ J. The data is fit with a threshold-linear function with intercept of 0.44 μ J and slope of 8.7 ± 3.4 pL/ μ J (mean and 0.95 CI) and (h) thrombus volume fractions, i.e., volume normalized to the volume of a sphere whose radius equals that of the vein; reanalysis of the data in panel G. The response at 0.5 μ J is statistically different from zero ($p < 0.01$) as is the response at 1.0 μ J ($p < 0.001$). The data is fit with a threshold-linear function, with intercept forced to be 0.77 μ J, for a slope of 0.17 ± 0.05 μ J⁻¹.

volume and platelet aggregates fraction at 650 s differed significantly across different control and *D*-glucose groups.

Results

To test whether hyperglycemia in isolation exacerbates a thrombo-inflammatory response to vascular tissue disruption, we examined responses in cortical veins of wild type mice where paired injuries are performed in a blinded fashion in the same subject under hyperglycemic, i.e., *D*-glc or normoglycemic, i.e., *L*-glc, challenge. Pharmacological manipulations to blunt hyperglycemic pathogenic pathways in transiently hyperglycemic mice were tested for their effects on mitigation of the laser-triggered vascular tissue disruption. As controls, we utilized two models of murine diabetes to establish a baseline standard for the response to vascular tissue disruption in the presence of comorbidities linked to diabetes. All data was taken from pial venules above parietal cortex.

Cerebrovascular mapping

We map the topology of a fluorescent-gel filled pial venule network (11 vessels across 5 mice; Figure 1(a)). In agreement with past claims,³² we find that the topology of all venules appear as tree; this is unlike the pial arterioles, which form loops⁴³ (Figure 1(a)). We chose 3rd or 4th order branches as target venules.

Venule laser targeting

Veins were visualized from plasma pool labeling with Texas red dextran (Figure 1(b)) while platelets were fluorescently labeled by injection of AF594-conjugated anti-CD41 antibodies (Figure 1(c)). To visualize neutrophil/leukocyte responses to laser-induced disruption, we utilized transgenic LysM-eGFP mice whose blood leukocytes are endogenously labeled through expression of eGFP.

Targeted laser-induced disruption to the lumen of a venule was delivered by amplified ultra-short laser pulses of known energy.²⁷ Real time changes in fluorescence were continuously recorded and normalized to baseline pre-perturbation levels to quantify the dynamic effects of laser-induced disruption across a ROI centered around the blood vessel in a single imaging plane. We tested the effect of laser pulse energies ranging from 0.1 μ J to 2.0 μ J (Figure 1(d) to (h)). Laser-induced disruption led to a sharp peak in the aggregation of fluorescent platelets. The amplitude in fluorescence decayed from its peak value, post-disruption, towards a plateau value after 400 s of recovery (Figure 1(e)). We reconstructed the volume of the platelet-rich thrombi during the plateau period from successive optical

sections (Figure 1(f) and (g)). Thrombus volumes increased with increasing of laser pulse energies. The first statistically significant change from zero volume occurs at an energy of 0.5 μ J ($p < 0.01$; Figure 1(g)), for which we observe thrombi with a mean volume of 0.41 pl (0.08 to 1.02 pl, 0.95 confidence interval (CI)). However, despite the statistical significance, there were cases with no thrombi. At 1.0 μ J per pulse, thrombi formed in all cases and thus we use 1.0 μ J per pulse in all experiments going forward. Here the mean volume of the thrombus is 2.5 pl (1.7 to 4.1 pl). As a normalized metric, we estimated the measured thrombus volume relative to that of the volume for a hypothetical sphere whose diameter equals the diameter of the vessel (Figure 1(h)). We designate this quantity as the “thrombus volume fraction”. The mean thrombus volume fraction at 1.0 μ J per pulse is small, i.e., 0.071 (0.038 to 0.134), so that the thrombi we form are modest in size. Lastly, we inferred the extent of serum extravasation from the fluorescence of extravascular labeled serum within seconds after irradiation (Figure 1(d) and (e)).

In total, these test data highlight the quantitative relation between laser pulse energies and intra- and juxta-luminal responses to vascular tissue disruption. It sets the stage for the use of this targeted assay to assess the increased susceptibility of venules to irradiation damage by hyperglycemia.

Effect of transient glucose spikes on systemic blood glucose, fibrinogen, and ROS

We first determined the window of time for a heightened level of blood glucose (Figure 2(a)). We varied the concentration of *D*-glc that we injected from 0.25 g/kg to 2.0 g/kg. In all cases, injection of *D*-glc results in a significant, transient increase in blood glucose concentration that peaks at 30 minutes and then returns to normal level after 120 minutes (Figure 2(b)). Thus, the laser injuries were performed 30 minutes after glucose injection. Further, an initial injection of 1.5 g/kg to 2.0 g/kg *D*-glc leads to blood glucose concentrations that exceed 300 mg/dl, the range of pathological hyperglycemia for non-fasting mice.⁴⁴ We note that mice injected with *L*-glc or with saline showed no significant changes in blood glucose levels (Figure 2(b)).

We tested for systemic effects of a spike of glucose in healthy animals using an injection of 2.0 g/kg *D*-glc. We assay PRP for reactive oxygen species (ROS) with the indicator MitoSOX red at the peak glucose level (Figure 2(b)). We observe a statistically significant, two-to-three-fold increase in ROS compared with control mice receiving saline injections (Figure 2(c)). We further tested for increased in fibrinogen, part of the known prothrombic pathways. Fibrinogen levels

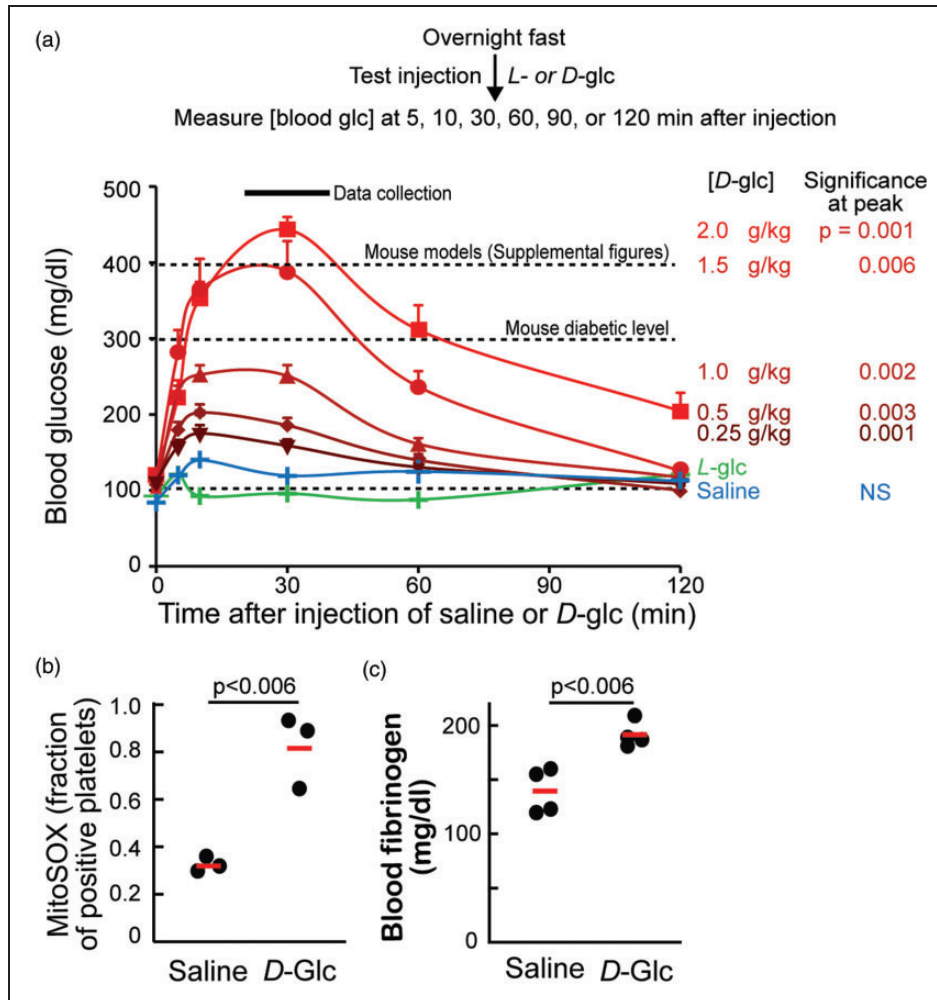


Figure 2. Blood glucose level measurements after injection of glucose into wild type mice. (a) Study design. Data was taken after the injection of saline (control; 6 mice), *L*-glc (inert control; 6 mice); or *D*-glc (metabolic glucose) at concentrations of 0.25 g/kg (9 mice), 0.5 g/kg (7 mice), 1.0 g/kg (8 mice), 1.5 g/kg (5 mice), and 2.0 g/kg (9 mice); 50 mice total. (b) Involvement of hyperglycemia in induction of ROS by platelets. Effect of *D*-glc injection on platelet production of superoxide were measured by flow cytometry using MitoSOX as an indicator of mitochondrial superoxide. Each circle represents a single mice treated with saline or *D*-glc (3 mice each). ($p < 0.006$). (c) Blood Fibrinogen level measurements after injection of saline or *D*-glc into wild type mice. Data was taken 30 minutes after the injection of saline (control; 4 mice) or *D*-glc at concentrations of 2.0 g/kg; 4 mice total. Blood fibrinogen concentration was determined using a blood coagulation analyzer.

significantly increased in response to an injection of 2.0 g/kg *D*-glc compared to saline control mice (Figure 2(d)).

Blinded study of vascular disruption from glucose spikes

Chronic hyperglycemia is associated with multiple morbidities that have been linked to vascular pathology.⁴⁵ Does transiently high blood glucose levels induce susceptibility to thrombus formation in response to vascular tissue disruption? Laser effects are first tested with a baseline dose of inert *L*-glc, which cannot be metabolized and which serves as osmotic

control. This was followed by laser disruption after a second injection of either *L*- or *D*-glc; the nature of the second injection remained blinded until after data analysis of fluorescence changes was completed (Figure 3 (a)).

For each injection of *L*- or *D*-glc, three pial venules were targeted for laser-induced disruption at energies of 0.2 μ J, 0.5 μ J, and 1.0 μ J each (Figure 3(b)). Platelet aggregation, at energies of 0.5 μ J and 1.0 μ J, and serum extravasation, at an energy of 0.5 μ J, were significantly greater after injections of *D*-glc as compared to tissue damage observed after injection of inert *L*-glc at the same level of laser energy (Figure 3(c) and (d)). Volumetric reconstruction of the thrombi and the

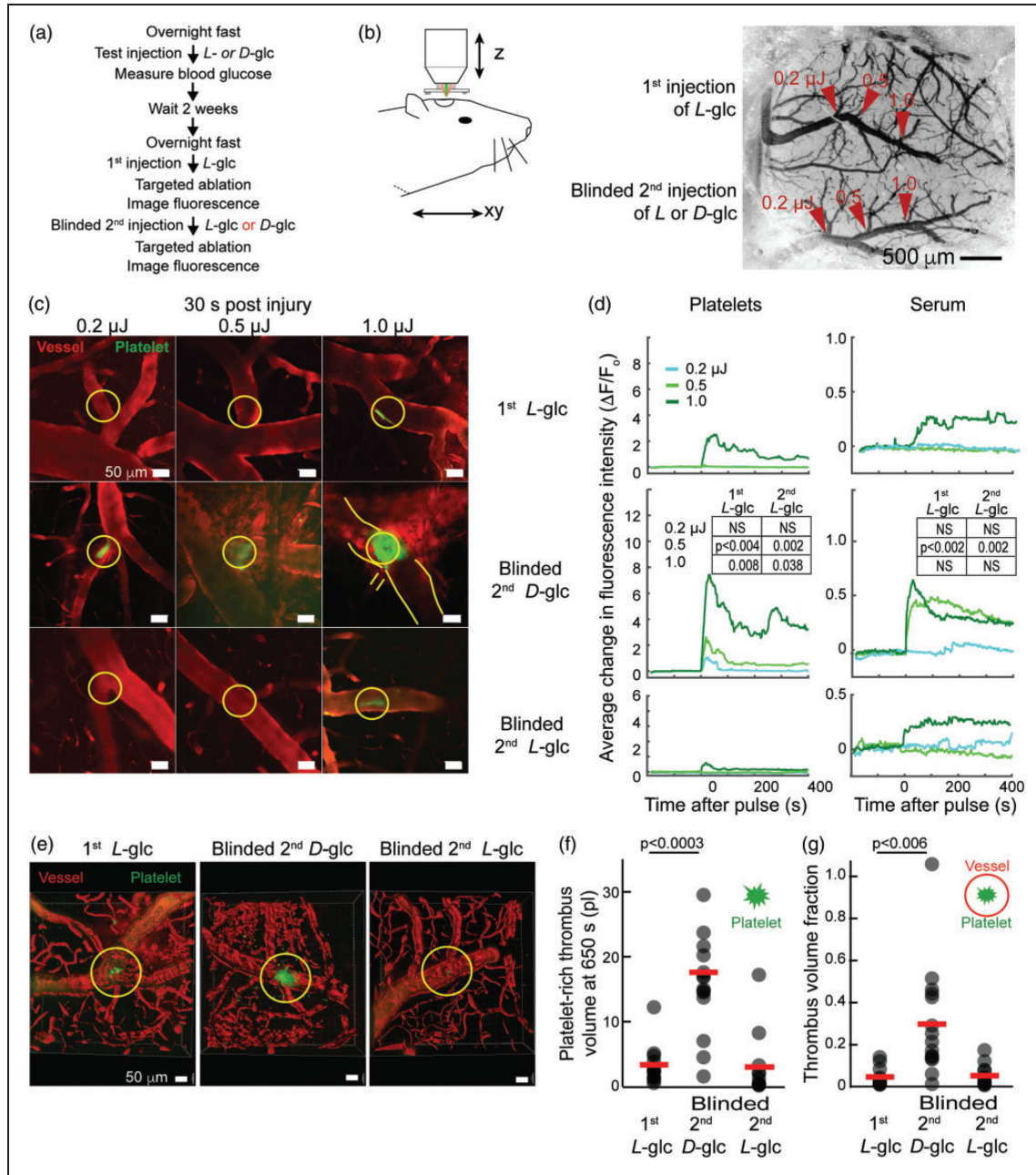


Figure 3. Double blinded study shows that transient hyperglycemia induced by injection of D-glucose but not L-glucose increases susceptibility to laser-induced vascular disruption. (a) Study design. (b) Schematic of set-up and image of surface vasculature of mouse cortex; arrow indicates branch of superior cerebral vein targeted with 0.2 μJ, 0.5 μJ, and 1.0 μJ laser energy, following treatment with 1st injection of 2nd injection of blinded L-glc (upper vein) or D-glc (lower vein). (c) Example images of platelet (green), and associated serum (red) fluorescence in cortical veins targeted by 0.2 μJ, 0.5 μJ, and 1.0 μJ laser pulses, 30 s post laser damage, in wild type mice treated with a 1st injection of L-glc and a 2nd, blinded injection of L- or D-glc. Site of focal damage is marked with yellow circle, along with the outline of the vein in selected images. (d) Effects of varying laser energy on the time course of the aggregation of platelets and blood extravasation induced by vascular disruption. Each curve is generated from the average change in vein fluorescence relative to baseline values. Each animal received a 1st injection of L-glc and a second injection of either L- or D-glc; 6 mice each for 12 mice total. A set of three veins per animal were irradiated 0.2 μJ, 0.5 μJ, and 1.0 μJ after the 1st L-glc injection and a second set was irradiated after the 2nd, blinded, injection. The insets give the Wilcoxon statistics for 1st L-glc and the blinded control 2nd L-glc relative to the experimental condition of the 2nd D-glc (averaged at 300–400 s post laser damage). (e) Three dimensional reconstructions of thrombi (green) within vasculature (red), collected 600 s post laser-induced vascular disruption. (f) Thrombi volumes at 600 s post laser-induced vascular disruption with 1.0 μJ irradiation. The red bar is the mean; 3.3 (2.2 to 6.1, 0.95 CI) pl for 1st L-glc; 17.6 (13.2 to 24.3) pl for 2nd D-glc. (g) Thrombus volume fraction at 600 s post laser-induced vascular disruption with 1.0 μJ irradiation. The red bar is the mean; 0.11 (0.08 to 0.14) for 1st L-glc; 0.28 (0.22 to 0.34) for 2nd D-glc. Continued.

associated thrombus volume fractions also showed a greater value when formed in conjunction with *D*-glc injections (Figure 3(e) to (g)). In terms of an analysis over all samples, the mean thrombus volume fraction for the *D*-glc injected mice was 0.30 (0.20 to 0.49), as compared with a mean volume fraction of 0.044 (0.024 to 0.076) for the first *L*-glc injection or a mean volume fraction of 0.050 (0.028 to 0.088) for the second *L*-glc injection; the difference between *D*- and *L*-glc is significant ($p < 0.0003$ for 1st and $p < 0.0006$ for 2nd *L*-glc; Figure 3(g)). These data indicate that a transient elevation in the concentration of blood glucose, renders healthy mice significantly more susceptible to laser induced platelet aggregation.

Impact of sub-pathological as well as pathological blood glucose levels on susceptibility to disruption

To establish the susceptibility of vessels to laser-induced disruption, our double-blind experiments (Figure 3) made use of a spike in blood glucose (Figure 2) that is comparable to the hyperglycemia observed in diabetic mice models (Supplemental Figures 1A and 2B). We now address how blood glucose spikes of lower magnitudes affect the cerebrovascular thrombo-inflammatory response. Injections of *D*-glc ranged from 0.25 g/kg to 2.0 g/kg led to peak blood levels of 170 mg/dl to 440 mg/dl blood glucose respectively (Figures 2 and 4(a) and (b)). Second injections of saline control served as controls (Figure 4(a)). For each pair of injections of saline and *D*-glc, three pial venules were targeted for laser disruption with 1.0 μ J laser pulses (Figure 4(b)). We observe that platelet aggregation and serum extravasation were significantly greater than baseline after injections of *D*-glc at all concentrations greater than 0.5 g/kg (Figure 4(c) and (d)); only injection of *D*-glc at a concentration of 0.25 g/kg did not lead to significant, excessive damage (Figure 4(c) and (d)).

Volumetric reconstruction of the platelet-rich thrombi and the associated thrombus volume fractions showed a greater value when formed in conjunction with *D*-glc injections (Figure 4(e) and (f)). In the *D*-glc injected mice the average thrombus volume fraction was significantly different compared to saline control for injections of 1.0 g/kg, (mean thrombus fraction

0.057 (0.029 to 0.098), $p < 0.04$), 1.5 g/kg (mean thrombus fraction 0.18 (0.08 to 0.33), $p < 0.0006$), and 2.0 g/kg (thrombus fraction 0.24 (0.18 to 0.31), $p < 0.0006$) (Figure 4(g)).

All told, these data (Figures 2 and 4(d), (f) and (g)) indicate even glucose spikes that are sub-pathological increase susceptibility to laser induced platelet aggregation and serum extravasation.

Diminution of damage by suppression of platelet activation

Thrombo-inflammation, as the immediate response to vascular tissue disruption, also includes neutrophil activation and recruitment.⁴⁶ We therefore extended our analyses of the effects of transient hyperglycemia on vascular tissue disruption to specifically monitor the neutrophil responses in LysM-eGFP mice, in which blood myelomonocytic cells and in particular neutrophils are endogenously fluorescently labeled.⁴⁷ Mice were successively split into four cohorts to test the effect of blocking platelet mediated neutrophil activation (Figure 5(a)). In the first split, mice were i.p. injected with clopidogrel, an adenosine diphosphate receptor P2Y₁₂ blocker that acts to suppress platelet hyperactivation, or they were injected with saline as a control. The second split was by an injection of either *L*- or *D*-glc (Figure 5(b)).

In the absence of inhibitor, we observed that the *D*-glc injected mice developed platelet aggregates that were significantly larger than those in *L*-glc injected mice (Figure 5(c) and (d)). This is consistent with the previous, fully blinded experimental result (Figure 3(d)). Neutrophil recruitment was also significantly greater in the *D*-glc treated mice, with a linear growth of neutrophil binding (slope = $0.0023 \pm 0.0002 \text{ s}^{-1}$, mean and 0.95 CI; Figure 5(d)). Critically, pretreatment with the platelet inhibitor clopidogrel significantly reduced platelet aggregation and neutrophil recruitment in *D*-glc injected mice (Figure 5(c) and (d)). Pretreatment with clopidogrel also inhibited serum extravasation (Figure 5(c) and (d)). Volumetric reconstruction of platelet and neutrophil aggregation indicated significantly greater volumes in the *D*-glc injected mice as compared to *L*-glc injected mice and as compared to *D*-glc injected mice with clopidogrel

Figure 3. Continued.

for 2nd *D*-glc; and 3.0 (1.2 to 7.8) pl for 2nd *L*-glc. For the first injection with *L*-glc the value does not differ from the baseline value of Figure 1(g) ($p = 0.62$). For the second injection with *D*-glc the value significantly differs from the baseline value ($p < 0.0003$). For the second injection with *L*-glc the value does not differ from the baseline value ($p = 0.31$). (g) Thrombus volume fractions for 1.0 μ J irradiation; reanalysis of the data in panel F. The red bar is the mean; 0.044 (0.024 to 0.076) for 1st *L*-glc; 0.30 (0.21 to 0.49) for 2nd *D*-glc; and 0.050 (0.028 to 0.089) for 2nd *L*-glc. For the first injection with *L*-glc the value does not differ from the baseline value of Figure 1(h) ($p = 0.53$). For a second injection with *D*-glc the value significantly differs from the baseline value ($p < 0.006$). For a second injection with *L*-glc the value does not differ from the baseline value ($p = 0.67$).

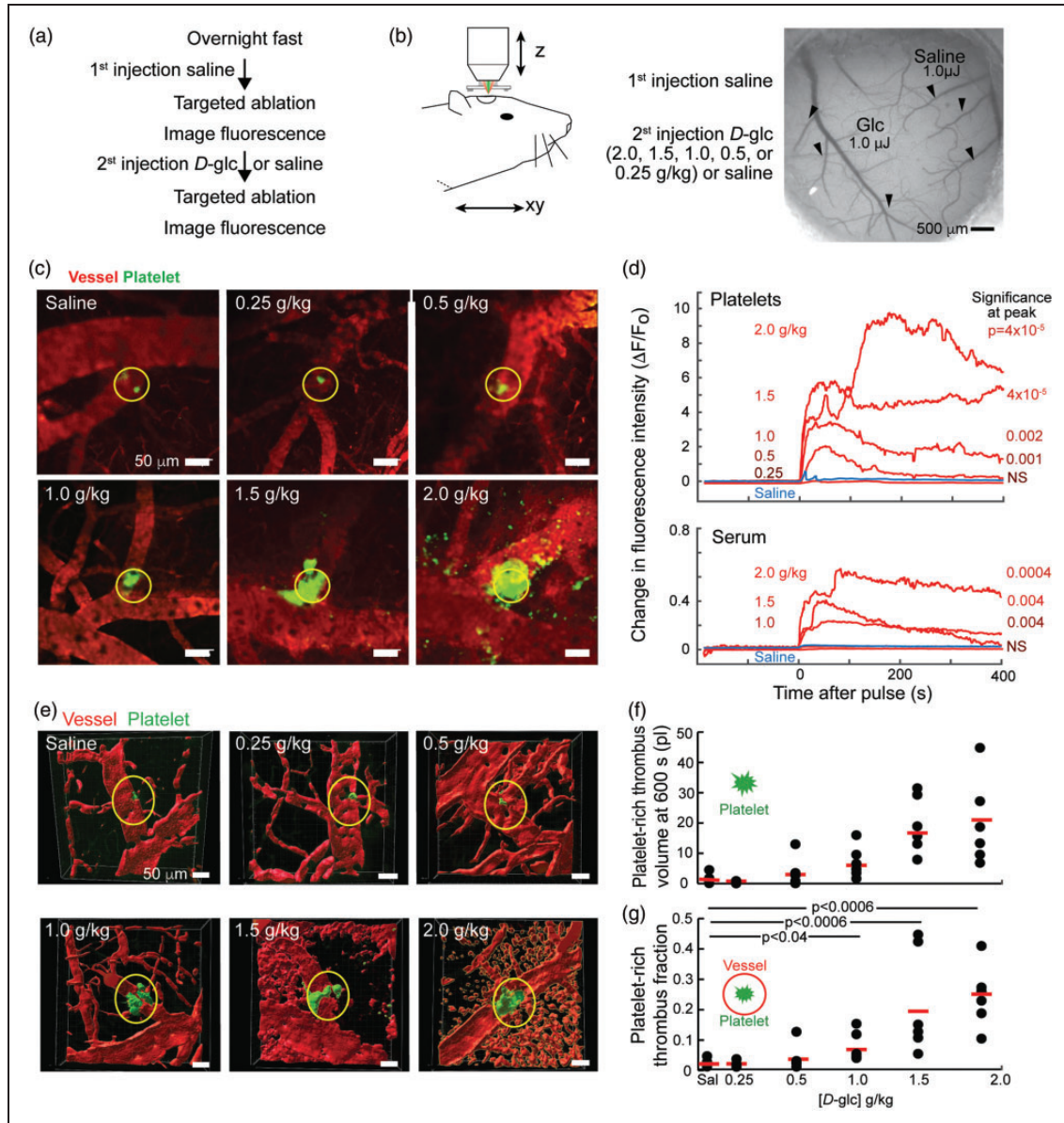


Figure 4. Normal, sub pathological and pathological blood glucose level effect on cerebrovascular susceptibility. (a) Study design. (b) Schematic of set-up and image of surface vasculature of mouse cortex; arrow indicates branch of superior cerebral vein targeted with 1.0 μ J laser energy, following treatment with 1st injection of saline and 2nd injection of D-glc, at 0.25, 0.5, 1.0, 1.5 or 2.0 g/kg, or a saline control. (c) Example images of platelet (green) and serum (red) fluorescence in cortical veins targeted with 1.0 μ J laser pulses, 30 s post laser-induced vascular disruption, in WT mice treated with a 1st injection of saline and a 2nd injection of D-glc in concentrations of 0.25, 0.5, 1.0, 1.5 and 2.0 g/kg. Site of focal damage is marked with yellow circle, along with the outline of the vein in selected images. (d) Effects of 1.0 μ J laser energy on the time course of aggregation of platelets and blood extravasation. Each curve is generated from the average change in vein fluorescence relative to baseline values. Each animal received a 1st injection of saline and a second injection of D-glc. A set of three or four veins per animal for were irradiated at 1.0 μ J after the 1st saline injection and after a second injection of 0.25, 0.5, 1.0, 1.5, or 2.0 g/kg D-glc; 3 mice each for 15 mice total. As a control, a set of three veins per animal for were irradiated at 1.0 μ J after both a 1st saline injection and a 2nd saline; 12 mice total. The grand total is 27 mice. (e) Three-dimensional reconstructions of thrombi (green) within vasculature (red), collected 600 s post laser-induced vascular disruption. (f) Thrombus volumes at 600 s post laser-induced vascular disruption. The red bar is the mean; only 7 of the 12 saline controls were used. For the injection with saline the value does not differ from the baseline value of Figure 1 (g) and (g) Thrombus volume fractions; reanalysis of the data in panel G. The red bar is the mean.

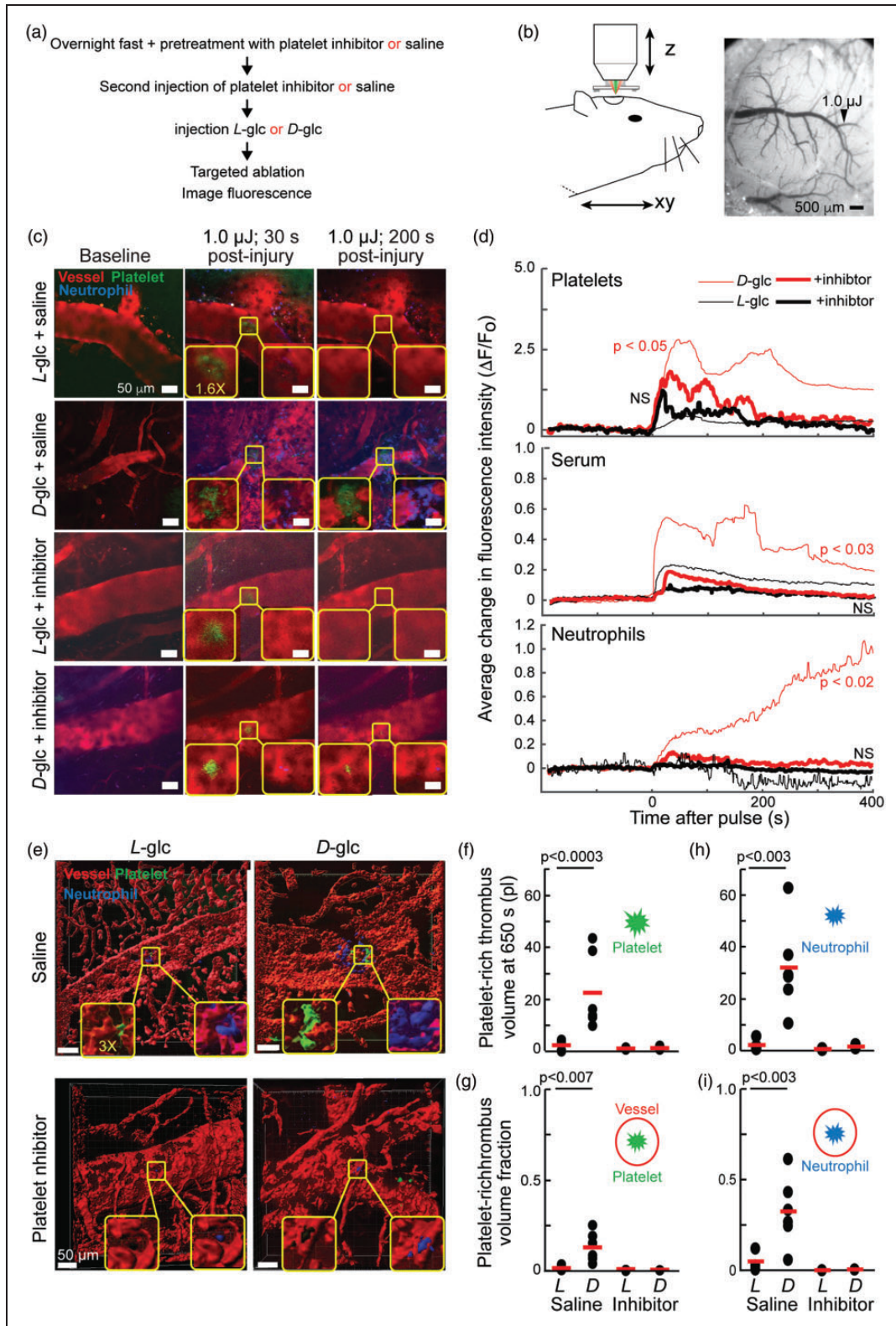


Figure 5. Transient hyperglycemia induced by D-glucose but not by L-glucose injection increases neutrophil recruitment following laser-induced vascular disruption. (a) Study design using lysM-eGFP mice with genetically labeled neutrophils. (b) Schematic of set-up and image of surface vasculature; arrow indicates branch of superior cerebral vein targeted with laser, following pretreatment with platelet inhibitor or saline followed by injection of L- or D-glc. (c) Example images of platelet (green), neutrophil (blue) and serum (red) fluorescence in cortical veins targeted with laser pulses in mice pretreated with saline, followed by injection of L- or D-glc, or Continued.

(Figure 5(e) and (f)). In the *D*-glc injected mice the platelet aggregates led to a mean thrombus volume fraction of 0.084 (0.048 to 0.131), significantly higher than in the *L*-glc injected mice ($p < 0.004$) albeit not higher than baseline control (Figure 1(h)). Similarly, the neutrophil aggregates occupied a mean volume fraction of 0.32 (0.20 to 0.46), which is significantly higher than in the *L*-glc injected mice ($p < 0.009$); the relatively large volume results from the continued recruitment of neutrophils over the course of the measurements (Figure 5(d)) and the large size of neutrophils relative to that of platelets. Platelet inhibitor treatment greatly diminished the aggregation of platelets for the *D*-glc injected mice, with the mean thrombus volume fraction reduced to 0.0034 (0.0015 to 0.0045) (Figure 5(f) and (g)), as well as aggregation of neutrophils (Figure 5(h) and (i)), with the mean thrombus volume fraction reduced to 0.0051 (0.0023 to 0.0069) (Figure 5(i)); both changes are significant with $p < 0.03$.

In total, we found that transient hyperglycemia-activated platelet aggregates provide a nucleation point for neutrophils.

Diminution of damage by scavenging of reactive oxygen

A known complication of diabetes is the elevated production of reactive oxygen species (ROS).⁴⁸ Excessive

concentrations of ROS can hyperactivate platelets by depleting homeostatic vascular NO to form peroxynitrite.⁴⁹ Further hyperglycemia by itself results in systemic elevations of ROS (Figure 2(b) and (c)). We asked if the effects of transient hyperglycemia are blunted by administration of a mitochondria-targeted antioxidant Mitotempo, which is a ROS scavenger, and S-nitroso-N-acetyl-*DL*-penicillamine (SNAP), which is a nitric oxide (NO) donor. Mice were successively divided into six cohorts to test the effect of scavengers (Figure 6(a)). In the first split, wild type mice were i.p. injected with Mitotempo, with SNAP, or with saline as a control. The second split was by an injection of either *L*- or *D*-glc. We targeted a single pial vessel of each mouse with amplified laser pulses of 1.0 μ J (Figure 6(b)).

In the absence of antioxidants, we observed that the immediate acute response of *D*-glc injected mice was an increase in platelet aggregation and serum extravasation after a laser pulse as compared to the effects observed in the *L*-glc injected control mice (Figure 6(c) and (d)). Critically, pretreatment with Mitotempo or with SNAP reduced platelet aggregation and reduced serum extravasation in both *L*- and *D*-glc injected mice (Figure 6(c) and (d)). Volumetric reconstruction of platelet aggregates in the *D*-glc injected mice indicated that these volumes were significantly greater than platelet aggregate volumes in *L*-glc injected control mice (Figure 6(e) and (f)). In terms of an analysis over all samples, in the *D*-glc injected mice the mean

Figure 5. Continued.

pretreated with the platelet inhibitor clopidogrel followed by *L*- or *D*-glc. Site of focal damage is marked with yellow rectangle. (d) Effects of 1.0 μ J laser energy on the time course of laser-induced thrombi, neutrophil recruitment, and blood extravasation. We use 6 mice and one vein per mouse in the saline pretreatment group, followed with injection *L*- or *D*-glc (6 mice per group or 12 total), and 4 mice and one vein per mouse in the platelet inhibitor group, also followed with injection *L*- or *D*-glc (4 mice per group or 8 total); grand total of 20 mice. P-values refer to Wilcoxon statistics for the inhibitor effect on the initial platelet change and the steady-state serum extravasation and neutrophil recruitment for *L*-glc and *D*-glc. (e) Three-dimensional reconstructions of thrombi (green) and neutrophil (blue) within vasculature (red), collected 600 s post laser-induced vascular disruption. Same veins as in panel D (upper panel). The red bar is the mean: 1.83 (0.73 to 3.16, 0.95 Cl) pl *L*-glc + saline; 22.2 (12.8 to 35.2) pl for *D*-glc + saline; 0.42 (0.15 to 0.57) pl for *L*-glc + inhibitor; and 0.69 (0.28 to 0.93) pl for *D*-glc + inhibitor). For injection with *L*-glc plus saline the values do not differ from the baseline values of Figure 1(g) ($p = 0.49$). For injection with *D*-glc plus saline the thrombus volumes differ from the baseline value ($p < 0.0003$). For injection with *L*- or *D*-glc plus inhibitor the values are significantly less than baseline, with $p < 0.03$ for both cases. (g) Thrombus volume fractions; reanalysis of the data in panel F. The red bar is the mean: 0.0089 (0.0040 to 0.0154) for *L*-glc + saline; 0.13 (0.08 to 0.20) for *D*-glc + saline; 0.0010 (0.0002 to 0.0018) for *L*-glc + inhibitor; and 0.0026 (0.0007 to 0.0040) for *D*-glc + inhibitor). For injection with *D*-glc plus saline the value does not differ from the baseline values of Figure 1(h) ($p = 0.09$). For injection with *L*-glc and *L*- or *D*-glc plus inhibitor the values are significantly less than baseline, with $p < 0.03$, $p < 0.007$, and $p < 0.007$ respectively. The volume of the platelet aggregates after injection with *D*-glc is significantly greater than that with *D*-glc + inhibitor ($p < 0.03$). (h) Neutrophil aggregate volumes for post laser-induced vascular disruption. Same veins as in panel D. The red bar is the mean: 2.03 (1.14 to 4.00) pl for *L*-glc + saline; 31.8 (21.7 to 48.3) pl for *D*-glc + saline; 0.50 (0.13 to 0.75) pl for *L*-glc + inhibitor; and 1.50 (0.92 to 2.00) for *D*-glc + inhibitor. For injection with *D*-glc plus saline the value significantly differs from baseline ($p < 0.003$). For injection with *D*-glc plus inhibitor the values do not differ from baseline ($p = 0.71$). For injection with *L*-glc plus inhibitor the values are significantly less than baseline ($p < 0.05$). (i) Neutrophil aggregate volume fraction; reanalysis of the data in panel H. The red bar is the mean: 0.048 (0.012 to 0.101) for *L*-glc + saline; 0.32 (0.20 to 0.46) for *D*-glc + saline; 0.0007 (0.0004 to 0.0010) for *L*-glc + inhibitor; and 0.0050 (0.0023 to 0.0069) for *D*-glc + inhibitor). For injection with *D*-glc plus saline the value significantly differs from baseline ($p < 0.0018$). For injection with *D*-glc plus inhibitor the values do not differ from baseline ($p = 0.26$). For injection with *L*-glc plus inhibitor the values are significantly less than baseline ($p < 0.03$).

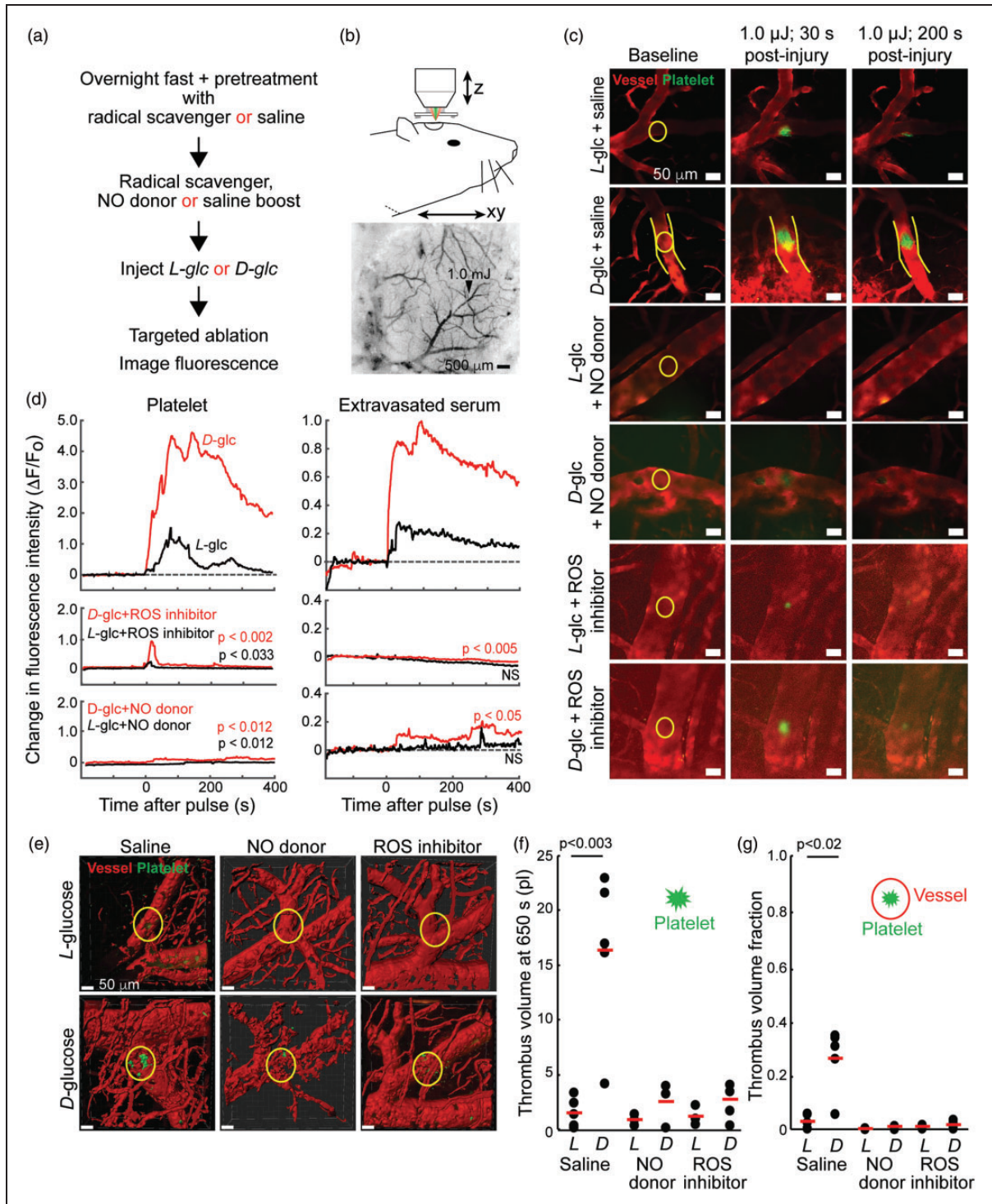


Figure 6. Involvement of hyperglycemia induced ROS and NO inhibition in susceptibility to laser-induced vascular disruption. (a) Study design. (b) Schematic of set-up and image of surface vasculature of mouse cortex; arrow indicates branch of superior cerebral vein targeted with 1.0 μJ laser energy, following pretreatment with NO donor, ROS scavenger or saline followed by injection of *L-* or *D-glc*. (c) Example images of platelet (green), and serum (red) fluorescence in cortical veins targeted with 1 μJ laser pulses, 0, 30 and 200 s post laser-induced vascular disruption in wild type mice pretreated and treated with saline, followed with injection *L-* or *D-glc*, or pretreated and treated with ROS scavenger (MitoTempo) followed by *L-* or *D-glc*, or treated with NO donor (SNAP) followed by *L-* or *D-glc*. Site of focal damage is marked with yellow circle, along with vein outline in some images. (d) Effects of 1.0 μJ laser pulses on the time course of laser-induced thrombi, neutrophil recruitment, and blood extravasation. Each curve is generated from the

Continued.

platelet volume fraction after laser-induced disruption was 0.26 (0.11 to 0.32), significantly higher than for *L*-glc injected control mice at 0.029 (0.007 to 0.051) ($p < 0.02$) (Figure 6(g)). Injection of the ROS inhibitor Mitotempo dramatically and significantly reduced the mean thrombus volume fraction to 0.010 (0.004 to 0.014), for the *D*-glc injected mice ($p < 0.008$) (Figure 6 (g)). These data are in agreement with past studies that connects ROS intermediates with cerebrovascular inflammation.⁵⁰ Further, injection of the NO donor SNAP significantly reduced the mean thrombus volume fraction to 0.016 (0.007 to 0.028) for the *D*-glc injected mice ($p < 0.008$) (Figure 6(g)). In total, these data suggest a mechanism, in which excessive blood glucose fuels ROS production. This, in turns depletes, homeostatic NO and links hyperglycemia to cerebrovascular thrombus formation and inflammation.

Models of chronic hyperglycemia

How does the venous response to laser-induced tissue disruption for transient hyperglycemic normal mice compare to that for established mouse disease models of diabetes? We investigated this for two mouse models. The first is a model of type 1 diabetes in which streptozotocin (STZ) injections have destroyed pancreatic β -cells⁵¹ (Supplemental Figure 1). Here, fasting blood glucose levels are high, of order 400 mg/dl (Supplemental Figure 1A). In control, nondiabetic mice blood glucose levels are normal, of order 100 mg/dl (Supplemental Figure 1A). The high blood glucose level in STZ mice could be transiently reduced with a single i.p. injection of insulin (1 U/kg equal to ~ 120 mg/dl) (Supplemental Figure 1A). We examined pial venule disruption during hyperglycemia and insulin normalization of hyperglycemia (Supplemental Figure 1B,1C).

Both platelet aggregation and serum extravasation were observable at the 1.0 μ J threshold level for disruption after the first saline injection and in cases with a second saline injection (Supplemental Figure 1D,E). However, injection with insulin significantly reduced irradiation triggered platelet aggregation and abrogated serum extravasation (Supplemental Figure 1D,E). Laser-induced tissue disruption produced platelet aggregates whose volume and volume fractions were significantly reduced, to near control levels, during insulin treatment (middle row, Figure 7(d) and (e)), when glucose levels are reduced to near normal levels (Supplemental Figure 1A). A similar reduction in thrombus volume during insulin treatment was observed (Supplemental Figure 1G,H). This effect is substantial; the average thrombus volume fraction was over three-times as large in STZ mice (0.22 (0.13 to 0.30); Supplemental Figure 1H) as compared to normoglycemic mice (0.071 (0.038 to 0.134); Figure 1(h)) and insulin controls (0.034 (0.023 to 0.046); Supplemental Figure 1H) and the reduction upon insulin treatment was statistically significant (Mann-Whitney U-test, $p < 0.02$).

To model type 2 diabetes, we made use of leptin-receptor knock-out *db/db* mice. These mice are significantly overweight (Supplemental Figure 2A) and display chronic high blood glucose levels (~ 320 mg/dl) as compared to control mice (~ 110 mg/dl) (Supplemental Figure 2B). This model of hyperglycemia cannot be reversed with insulin,⁵² which indicates insulin resistance. The effects of laser-induced disruption to venules, at pulse energies of 1.0 μ J, were compared between *db/db* hyperglycemic versus control mice with normal blood glucose (Supplemental Figure 2C,D). The dynamic responses in these two groups demonstrated

Figure 6. Continued.

average change in vein fluorescence relative to baseline values. We use 12 mice and one vein per mouse irradiated at 1.0 μ J in the saline group (+ *L*- or *D*-glc at 6 mice each). We use 8 mice and one vein per mouse irradiated at 1.0 μ J in the ROS scavenger group (+ *L*- or *D*-glc at 3 mice each). We use 8 mice and one vein per mouse irradiated at 1.0 μ J in the NO donor group (+ *L*- or *D*-glc at 4 mice each). The grand total is 28 mice. P-values refer to Wilcoxon statistics for treatments with ROS-inhibitor and NO-donor for *L*- and *D*-glc injected mice relative to untreated. We computed statistics for the initial platelet change and the steady-state serum extravasation. (e) Example three dimensional reconstructions of thrombi (green) within vasculature (red), collected 600 s post laser-induced vascular disruption. (f) Thrombus volumes at 600 s post laser-induced vascular disruption. The red bar is the mean; 1.52 (0.45 to 2.58, 0.95 CI) pl for *L*-glc + saline; 16.4 (7.9 to 20.4) pl for *D*-glc + saline; 1.21 (0.45 to 1.80) pl for *L*-glc + NO donor; 2.76 (1.26 to 3.86) pl for *D*-glc + NO donor; 0.89 (0.38 to 1.22) pl for *L*-glc + ROS inhibitor; and 2.58 (1.10 to 3.69) pl for *D*-glc + ROS inhibitor. For the injection of *L*-glc the volume is consistent with baseline (Figure 1(g); $p = 0.31$), for injection of *D*-glc the volume differs from baseline ($p < 0.003$). For injection of either *L*- or *D*-glc plus NO donor the volume is consistent with baseline ($p = 0.29$ and $p = 0.68$, respectively). For injection of either *L*- or *D*-glc plus ROS inhibitor the volume is consistent with baseline ($p = 0.08$ and $p = 0.77$, respectively). (g) Thrombus volume fractions; reanalysis of the data in panel F. The red bar is the mean: 0.029 (0.007 to 0.051) for *L*-glc + saline; 0.26 (0.11 to 0.32) for *D*-glc + saline; 0.011 (0.003 to 0.016) for *L*-glc + NO donor; 0.016 (0.007 to 0.028) for *D*-glc + NO donor; 0.0025 (0.0010 to 0.0034) for *L*-glc + ROS inhibitor; and 0.010 (0.004 to 0.014) for *D*-glc + ROS inhibitor. For the injection of *L*-glc the volume fraction is consistent with baseline (Figure 1(g); $p = 0.21$), for injection of *D*-glc the fraction is greater than from baseline ($p < 0.02$). For injection of either *L*- or *D*-glc + NO donor the fraction is consistent with baseline ($p = 0.16$ for both). For injection of *D*-glc plus ROS inhibitor the volume is consistent with baseline ($p = 0.11$). For injection of *L*-glc plus ROS inhibitor the volume is significantly less than baseline ($p < 0.007$).

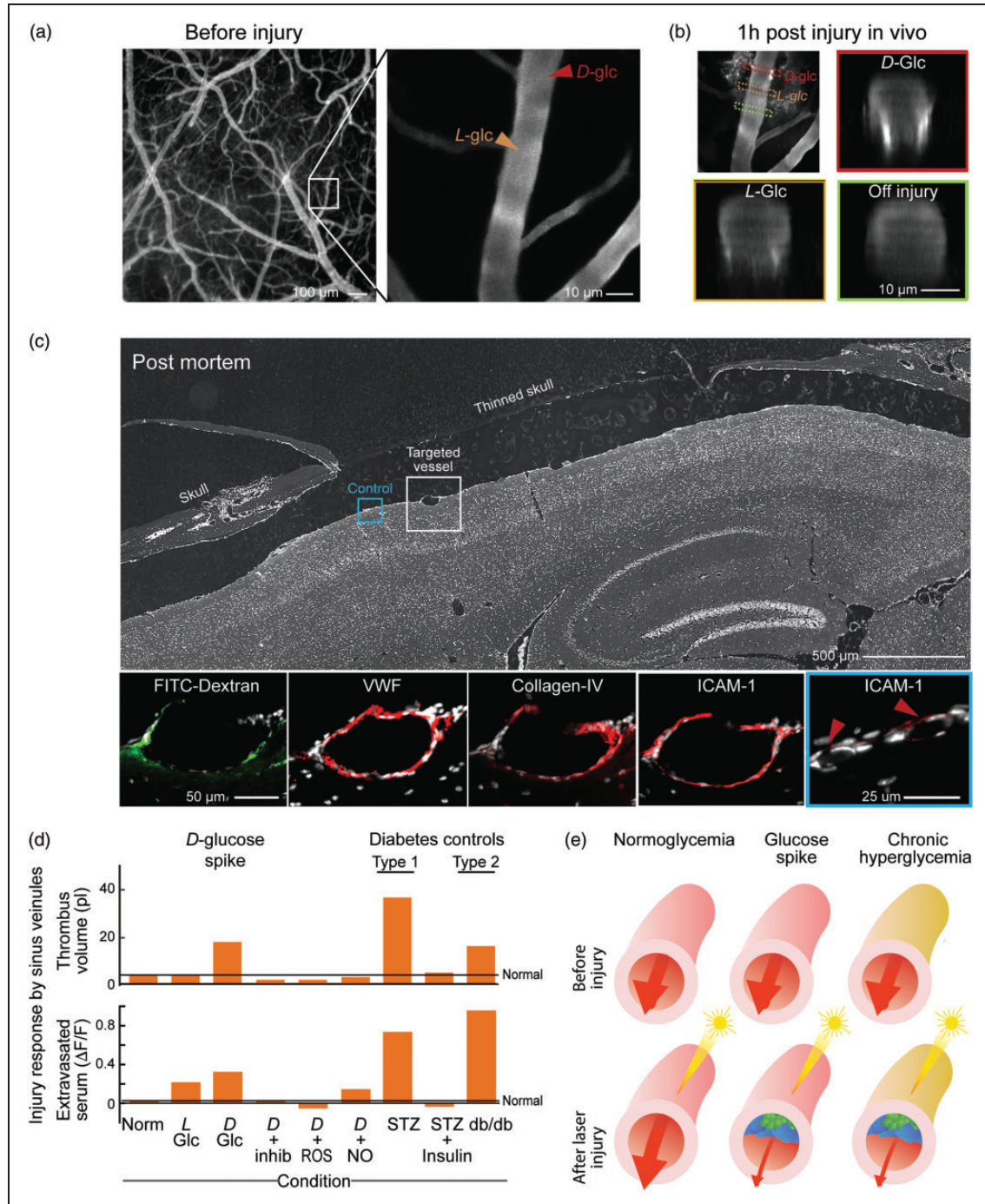


Figure 7. In vivo and post-mortem characterization of susceptibility to vessel perturbation in the presence of a transient hyperglycemia. (a) Wide-field image of the region of cortex prior to ablation shown on left and the maximal projection (90 μm) of an adaptive optics two-photon microscope image on the right to show intended target regions of a vein. The same ablation protocol was applied to two locations on a single vein segment, first 15 minutes after *L*-glc (yellow), and again 15 minutes after *D*-glc (red) injection. (b) In-vivo FITC accumulation as indicator of vessel wall damage. Localized FITC accumulation was evident ~ 1 hour later, again using adaptive optics for improved resolution. Orthogonal reconstructions of the healthy (green) and injured (red and yellow) vessel segments in the upper left-hand image locate the FITC accumulation to the proximity of the vessel wall. (c) Post-mortem histology. Top panel: Sagittal section of brain with laser targeted injured vein (white box), deep to thinned skull, and non-targeted vein (cyan box). Lower panels: Fluorescence images of three serial sections immunostained with activated endothelial cell markers: von Willebrand factor (VWF); collagen IV; intercellular adhesion molecule 1 (ICAM-1). Left most panel laser perturbed vessel from FITC-Dextran uptake by endothelial cells. Cytoplasmic immunostaining for each marker surrounds flat endothelial nuclei

Continued.

that there were significantly larger platelet aggregations and serum extravasation in the *db/db* mice as compared to normoglycemic mice (Supplemental Figure 2E,F). Volumetric reconstructions of platelet aggregates after laser-induced tissue disruption showed that obesity related hyperglycemia resulted in significantly greater aggregate volumes in *db/db* mice relative to control mice (Supplemental Figure 2G,H). In terms of an analysis over all samples, the mean thrombus volume fractions of platelet aggregates in *db/db* mice were 0.25 (0.11 to 0.40), which is significantly larger ($p < 0.04$) than the thrombus volume fractions for control normoglycemic mice (Figure 1(h) and Supplemental Figure 2I).

Characterization of the laser perturbation site under transient hyperglycemia

To test for vessel wall damage induced by targeted laser perturbation, we injected 2MD FITC-dextran intravenously and acquired a three-dimension set of images before and after laser perturbation of a vein using adaptive optics for improved spatial resolution⁴⁰ (Figure 7(a)). Axial reconstructions of the one-hour post-perturbation stack revealed focally increased FITC uptake in proximity to the perturbation sites. This indicates a localized vessel wall lesion (Figure 7(b)), consistent with previous reports of FITC uptake into the vessel wall⁵³ after transient ischemic injury.

In vivo responses to laser irradiation of veins are evident from platelet aggregation within the damaged vessel and serum extravasation emanating from vessel leakage sites adjacent to platelet clot (Figures 3 to 6). To obtain direct evidence of endothelial cell activation to laser irradiation, veins with in vivo signposts of damage under a glucose spike were examined. The signposts of in vivo damage include 2 MD FITC-dextran accumulation⁵³ (Figure 7(c)), and/or accumulation of CD41 immunofluorescent platelets (Supplemental Figure 4). Immunostaining of individual targeted veins examined in serial section allowed localization of multiple endothelial activation markers. Release of the glycoprotein von Willebrand Factor (VWF) from endothelial cell Weibel-Palade bodies, with the result of platelet aggregation to stem bleeding, is observed to characterize the acute phase activation.^{34,54–56} Here we observe VWF immunoreactivity in laser targeted veins (Figure 7(c) and Supplemental Figure 4).

Synthesis of the glycoprotein intercellular adhesion molecule 1 (ICAM-1)^{57–59} in activated endothelial cells in conjunction with elevations in serum fibrinogen (Figure 2(d)) can enhance platelet binding to injured vein endothelial cells⁶⁰ (Figure 2(d)). We observe densely immunoreactive ICAM-1 endothelial cells in laser perturbed veins (Figure 7(c) and Supplemental Figure 4). Gene mutation in Collagen-IV has been linked to perinatal cerebral hemorrhage⁶¹ and disruption of Factor IX binding to collagen IV in knock-in mice and supports a role for Collagen IV in normal hemostasis.⁶² We observe elevated Collagen IV immunoreactivity in laser perturbed vein endothelial cells (Figure 7(c) and Supplemental Figure 4). As a control, non-targeted vessels on these immunostained sections show only scant immunoreactivity for ICAM-1, VWF or Collagen IV antibodies (lower right-hand ICAM-1 panel Figure 7(c) and Supplemental Figure 4).

Meta-analysis of normoglycemia and transient hyperglycemia results

We purposely conducted separate controls for each set of experimental conditions to minimize potential systematic variability between experiments, such as may occur with different litters of mice despite matching for age and sex. This yielded multiple sets of control experiments that involved the same or nearly the same conditions. We considered a meta-analysis across experimental groups based on a one-way Kruskal–Wallis H-test. For the control condition of solely wild type animals (Figure 1) or wild type plus saline injection (Figure 4 and Supplemental Figure 2), we could not reject the null hypothesis, i.e., their mean values were not significantly different, yielding a mean thrombus volume fraction of 0.053 (0.033 to 0.095; 25 mice). For the control condition of wild type animals injected with *L*-glc (Figures 3, 5, and 6), we found that the combined results did not differ significantly from each other ($p < 0.12$), yielding a mean thrombus volume fraction of 0.032 (0.020 to 0.052; 23 mice). In fact, the data across all control groups do not differ significantly from each other and yield a grand mean thrombus volume fraction of 0.041 (0.030 to 0.062; 48 mice).

A similar meta-analysis was performed for all wild type animals injected with 2.0 g/kg of *D*-glc ($p < 0.91$;

Figure 7. Continued.

and delineates the reactive vessel wall in serial sections. Right panel shows sparsely immunostained vessels from same section with dense ICAM-1 staining of the laser perturbed vessel. This vessel segment is out of range of laser targeting (cyan rectangle in top panel) as it is deep to the thick part of the skull. The sparse ICAM-1 staining (red arrowheads), is consistent with known low constitutive expression of ICAM-1 in endothelial cells. (d) Summary of perturbation model for transient versus chronic hyperglycemia. Shown are the combined effects of 1.0 μ J ultra-short, pulsed laser energy on the peak of laser-induced of platelet fluorescence and the peak of laser-induced of serum extravasation fluorescence and (e) Graphical summary of our results.

Figures 3 to 6), but no subsequent pharmacological agents. We found a mean thrombus volume fraction of 0.28 (0.22 to 0.38; 29 mice), i.e., approximately seven-times the size of the thrombus under control conditions and significantly different ($p < 5 \times 10^{-8}$).

Plots of the diameters of veins as a function of experimental manipulation and groupings demonstrate no bias in selection of veins for targeted laser disruption (Supplemental Figure 3).

Discussion

Here we test the effect of a lone, transient spike in blood glucose on susceptibility to clotting in cortical veins in healthy mice. Venous clotting susceptibility was assessed using a reproducible targeted laser illumination to produce a precisely timed and precision focused perturbation through a thinned skull preparation in the awake animal (Figure 1). This experimental setup supports real-time imaging of dynamics of serum extravasation, platelet aggregation, and neutrophil aggregation in the injured vein. The essential data is based on a fully blinded experimental design and reveals that a single spike of increased blood *D*-glucose (Figure 2), but not of inert *L*-glucose, is sufficient to dramatically increase the platelet-rich thrombotic response to laser-induced focal perturbation to a vein (Figure 3). This suggests that the susceptibility to vascular thrombo-inflammation is heightened by transient hyperglycemia, even at levels of blood glucose, e.g., 1 g/kg *D*-glc dosage, that are below the fasting glucose diabetic threshold in mice (Figures 2 and 4).

The extent of extravasated serum from laser injured veins is well above control levels, but less than that for the diabetes models (Figure 7(d)). Surprisingly, the extent of thrombi clot volumes in animals, with transient hyperglycemia, rivals that for the diabetes models (Figure 7 and Supplemental Figures 1 and 2) even though the transiently hyperglycemic mice are otherwise healthy and lacking comorbidities.

What is the mechanism of heightened sensitivity to vascular damage in transient hyperglycemia? Acute hyperglycemia has been shown to increase platelet stickiness in harvested platelets of healthy and diabetic humans.⁶³ Here we found that pretreatment with a platelet inhibitor also is protective from effects of laser perturbation of veins in mice with a transient spike in blood glucose⁶⁴ (Figure 5). This abrogation of susceptibility indicates that platelet activation plays a key role.

A contributory role for vessel endothelial cells in conferring susceptibility is suggested by increased production of ROS by endothelial cells when stimulated by high glucose under chronic hyperglycemia.¹² Elevation of ROS species decreases bioavailability of NO, a coagulation cascade inhibitor.⁶⁵ An involvement of

ROS generation in transient hyperglycemia is supported by our observations of elevated ROS levels in plasma rich platelet fractions harvested from healthy mice subjected to transient hyperglycemia (Figure 2). Direct evidence for ROS/NO involvement is demonstrated by our observations that interference with ROS pathways and NO donor supplementation both reduce thrombi formation and extravasation in response to laser perturbation of veins in mice with transient hyperglycemia (Figure 6).

Chronic hyperglycemia in diabetic patients is linked to increased blood fibrinogen levels,⁶⁶ another risk factor for thrombosis. Healthy mice with transient hyperglycemia also show significant elevations in blood fibrinogen and notably this is independent of comorbidities (Figure 2). These systemic pro-thrombotic changes linked to transient hyperglycemia are likely to contribute to heightened susceptibility to laser-induced vein thrombosis that we observe in this study.

The results of the current study, combined with past *in vitro* studies,¹² supports a hypothesis that hyperglycemia, whether it is chronic or transient, facilitates platelet thrombus formation in response to vascular tissue disruption (Figure 7(e)). We introduce a mouse model comprised of two insults, i.e., transient hyperglycemia (Figure 2) and targeted laser perturbation (Figure 1), that consistently induce cerebral venous thrombosis. The reliability and reproducibility of this mouse model make it possible to quantify metrics for thresholds for each insult. This can support testing of other interventions that might reduce susceptibility, i.e., antioxidant dietary strategies.⁶⁷ It is tempting to speculate if the study of two insults in human patients, i.e., the conjunction of transient hyperglycemia along with any source of brain vascular damage, could reveal increased risk for cerebral venous thrombosis.

Funding

The author(s) disclosed receipt of the following financial support for the research, authorship, and/or publication of this article: This work was sponsored by National Institutes of Health grants R01 NS108472 and R35 NS097265 and the Swiss National Science Foundation grant P500PP_211149. Image analysis was performed at the UCSD School of Medicine Microscopy Core, funded by National Institutes of Health grant P30 NS047101.

Acknowledgements

We thank Sandra Black for introducing us to the biomedical importance of pathologies in cortical venules, Marta Koch, Dorian McGavern, Helena Shaked, Orian Shirihi and Bart Weijts for discussions, Celine Mateo for assistance with data analysis, Rodolfo Figueroa-Mercado for assistance with the blood glucose measurements, and Hannah Liechty for assistance with the fully blinded experimental design.

Declaration of conflicting interests

The author(s) declared no potential conflicts of interest with respect to the research, authorship, and/or publication of this article.

Authors' contributions

BF, DK and IS conceived the study. AD and DK secured funding. YC and XJ analyzed pial vasculature. CF, DK and RL constructed the in vivo experimental set-up. IS performed the in vivo imaging experiments with the assistance of TB and PM. SJ, TK and IS performed the blood analyses. CF performed all statistical tests. BF, MF, DK, IS and PS discussed and organized the results. BF, DK and IS wrote the manuscript. DK attended to the myriad of university rules and forms that govern environmental health and safety, including the ethical use of animals as well as the use of chemicals, controlled substances, hazardous substances, and lasers.

Supplementary material

Supplemental material for this article is available online.

References

- Fuentes B, Pastor-Yborra S, Gutierrez-Zuniga R, et al. Glycemic variability: prognostic impact on acute ischemic stroke and the impact of corrective treatment for hyperglycemia. The GLIAS-III translational study. *J Transl Med* 2020; 18: e414.
- Gonzalez-Moreno EI, Camara-Lemarroy CR, Gonzalez-Gonzalez JG, et al. Glycemic variability and acute ischemic stroke: the missing link? *Transl Stroke Res* 2014; 5: 638–646.
- Yoon JE, Sunwoo JS, Kim JS, et al. Poststroke glycemic variability increased recurrent cardiovascular events in diabetic patients. *J Diabetes Complications* 2017; 31: 390–394.
- El-Osta A, Brasacchio D, Yao D, et al. Transient high glucose causes persistent epigenetic changes and altered gene expression during subsequent normoglycemia. *J Exp Med* 2008; 205: 2409–2417.
- Hall H, Perelman D, Breschi A, et al. Glucotypes reveal new patterns of glucose dysregulation. *PLoS Biol* 2018; 16: e2005143.
- Qing H, Desrouleaux R, Israni-Winger K, et al. Origin and function of stress-induced IL-6 in murine models. *Cell* 2020; 182: 372–387.e14.
- van der Kooij MA, Jene T, Treccani G, et al. Chronic social stress-induced hyperglycemia in mice couples individual stress susceptibility to impaired spatial memory. *Proc Natl Acad Sci U S A* 2018; 115: E10187–E10196.
- Beckman JA, Creager MA and Libby P. Diabetes and atherosclerosis: epidemiology, pathophysiology, and management. *Journal of the. JAMA* 2002; 287: 2570–2581.
- Brzoska T, Vats R, Bennewitz MF, et al. Intravascular hemolysis triggers ADP-mediated generation of platelet-rich thrombi in precapillary pulmonary arterioles. *J Clin Investig Insight* 2020; 5: e139437.
- van der Meijden PEJ and Heemskerk JWM. Platelet biology and functions: new concepts and clinical perspectives. *Nat Rev Cardiol* 2019; 16: 166–179.
- Kraakman MJ, Lee MK, Al-Sharea A, et al. Neutrophil-derived S100 calcium-binding proteins A8/A9 promote reticulated thrombocytosis and atherogenesis in diabetes. *J Clin Invest* 2017; 127: 2133–2147.
- Nishikawa T, Edelstein D, Du XL, et al. Normalizing mitochondrial superoxide production blocks three pathways of hyperglycaemic damage. *Nature* 2000; 404: 787–790.
- Cai H and Harrison DG. Endothelial dysfunction in cardiovascular diseases: the role of oxidant stress. *Circ Res* 2000; 87: 840–844.
- Geraldes P, Hiraoka-Yamamoto J, Matsumoto M, et al. Activation of PKC-Delta and SHP-1 by hyperglycemia causes vascular cell apoptosis and diabetic retinopathy. *Nat Med* 2009; 15: 1298–1306.
- Ungvari Z, Tarantini S, Kirkpatrick AC, et al. Cerebral microhemorrhages: mechanisms, consequences, and prevention. *Am J Physiol Heart Circ Physiol* 2017; 312: H1128–H1143.
- Lindauer U, Megow D, Matsuda H, et al. Nitric oxide: a modulator, but not a mediator, of neurovascular coupling in rat somatosensory cortex. *Am J Physiol – Heart Circulatory Physiology* 1999; 277: 799–811.
- Naseem KM and Roberts W. Nitric oxide at a glance. *Platelets* 2011; 22: 148–152.
- Sreeramkumar V, Adrover JM, Ballesteros I, et al. Neutrophils scan for activated platelets to initiate inflammation. *Science* 2014; 346: 1234–1238.
- Falati S, Gross P, Merrill-Skoloff G, et al. Real-time in vivo imaging of platelets, tissue factor and fibrin during arterial thrombus formation in the mouse. *Nat Med* 2002; 8: 1175–1181.
- Versteeg HH, Heemskerk JWM, Levi M, et al. New fundamentals in hemostasis. *Physiol Rev* 2013; 93: 327–358.
- Stark K and Massberg S. Interplay between inflammation and thrombosis in cardiovascular pathology. *Nat Rev Cardiol* 2021; 18: 666–682.
- Blanc L and Lordkipanidzé JM. Platelet function in aging. *Frontiers of Cardiovascular Medicine* 2019; 6: e109.
- Loesel FH, Fischer JP, Gotz MH, et al. Non-thermal ablation of neural tissue with femtosecond laser pulses. *Appl Phys B* 1998; 66: 121–128.
- Tsai PS, Blinder P, Migliori BJ, et al. Plasma-mediated ablation: an optical tool for submicrometer surgery on neuronal and vascular systems. *Curr Opin Biotechnol* 2009; 20: 90–99.
- Lagraoui M, Latoche JR, Cartwright NG, et al. Controlled cortical impact and craniotomy induce strikingly similar profiles of inflammatory gene expression, but with distinct kinetics. *Front Neurol* 2012; 3: e155.
- Drew PJ, Shih AY, Driscoll JD, et al. Chronic optical access through a polished and reinforced thinned skull. *Nat Methods* 2010; 7: 981–984.
- Nishimura N, Schaffer CB, Friedman B, et al. Targeted insult to individual subsurface cortical blood vessels using ultrashort laser pulses: three models of stroke. *Nat Methods* 2006; 3: 99–108.

28. Nishimura N, Rosidi NL, Iadecola C, et al. Limitations of collateral flow after occlusion of a single cortical penetrating arteriole. *J Cereb Blood Flow Metab* 2010; 30: 1914–1927.
29. Koyama M, Minale F, Shum J, et al. A circuit motif in the zebrafish hindbrain for a two alternative behavioral choice to turn left or right. *eLife* 2016; 5: e16808.
30. Cheng Z, Han Y, Wei B, et al. Probing neuronal functions with precise and targeted laser ablation in the living cortex. *Optica* 2021; 8: 1559–1572.
31. Rustenhoven J, Drieu A, Mamuladze T, et al. Functional characterization of the dural sinuses as a neuroimmune interface. *Cell* 2021; 184: 1000–1016.e27.
32. Coelho-Santos V and Shih AY. Postnatal development of cerebrovascular structure and the neurogliovascular unit. *Wiley Interdiscip Rev Dev Biol* 2020; 9: e363.
33. Fisher MJ. Brain regulation of thrombosis and hemostasis. *Stroke* 2013; 44: 3275–3285.
34. Wagner DD and Frenette PS. The vessel wall and its interactions. *Blood* 2008; 111: 5271–5281.
35. Carvalho-Tavares J, Hickey MJ, Hutchison J, et al. A role for platelets and endothelial selectins in tumor necrosis factor- α -induced leukocyte recruitment in the brain microvasculature. *Circ Res* 2000; 87: 1141–1148.
36. Shih AY, Mateo C, Drew PJ, et al. A polished and reinforced thinned skull window for long-term imaging and optical manipulation of the mouse cortex. *JoVE* 2012; www.jove.com/video/3742.
37. Tsai PS and Kleinfeld D. In vivo two-photon laser scanning microscopy with concurrent plasma-mediated ablation: Principles and hardware realization. In: RD Frostig (ed.) *Methods for in vivo optical imaging*. 2nd edition. Boca Raton: CRC Press, 2009, pp. 59–115.
38. Tsai PS, Friedman B, Schaffer CB, et al. All-optical, in situ histology of neuronal tissue with femtosecond laser pulses. In: R Yuste and A Konnerth (eds) *Imaging in neuroscience and development: a laboratory manual*. Vol. 102. Cold Spring Harbor Laboratory Press, 2005, pp. 815–826.
39. Jeong DC, Tsai PS and Kleinfeld D. All-optical osteotomy to create windows for transcranial imaging in mice. *Opt Express* 2013; 21: 23160–23168.
40. Liu R, Li Z, Marvin JS, et al. Direct wavefront sensing enables functional imaging of infragranular axons and spines. *Nat Methods* 2019; 16: 615–618.
41. Kilkenny C, Browne WJ, Cuthill IC, et al. Improving bioscience research reporting: the ARRIVE guidelines for reporting animal research. *Public Library of Science Biology* 2010; 8: e1000412.
42. D’Errico J. SLM – Shape Language Modeling, www.mathworks.com/matlabcentral/fileexchange/24443-slm-shape-language-modeling. MATLAB Central File Exchange (2021, accessed 1 May 2022).
43. Blinder P, Shih AY, Rafie CA, et al. Topological basis for the robust distribution of blood to rodent neocortex. *Proc Natl Acad Sci U S A* 2010; 107: 12670–12675.
44. King AJF. The use of animal models in diabetes research. *Br J Pharmacol* 2012; 166: 877–894.
45. Schneider DJ. Abnormalities of coagulation, platelet function, and fibrinolysis associated with syndromes of insulin resistance. *Coron Artery Dis* 2005; 16: 473–476.
46. De Meyer SF, Denorme F, Langhauser F, et al. Thromboinflammation in stroke brain damage. *Stroke* 2016; 47: 1165–1172.
47. Faust N, Varas F, Kelly LM, et al. Insertion of enhanced green fluorescent protein into the lysozyme gene creates mice with green fluorescent granulocytes and macrophages. *Blood* 2000; 96: 719–726.
48. Volpe CMO, Villar-Delfino PH, Dos Anjos PMF, et al. Cellular death, reactive oxygen species (ROS) and diabetic complications. *Cell Death Dis* 2018; 9: e119.
49. Forstermann U, Xia N and Li H. Roles of vascular oxidative stress and nitric oxide in the pathogenesis of atherosclerosis. *Circ Res* 2017; 120: 713–735.
50. Olmez I and Ozyurt H. Reactive oxygen species and ischemic cerebrovascular disease. *Neurochem Int* 2012; 60: 208–212.
51. Wu KK and Huan Y. *In current protocols of pharmacology e47*. Hoboken: Wiley, 2008.
52. Chen H, Charlat O, Tartaglia LA, et al. Evidence that the diabetes gene encodes the leptin receptor: identification of a mutation in the leptin receptor gene in db/db mice. *Cell* 1996; 84: 491–495.
53. Chen B, Friedman B, Cheng Q, et al. Severe blood brain barrier disruption and surrounding tissue injury. *Stroke* 2009; 40: e666–674.
54. Moore KH, Murphy HA and George EM. The glycocalyx a central regulator of vascular function. *Am J Physiol-Regulatory, Integrative Comparative Physiol* 2021; 320: R508–R518.
55. Drakeford C, Aguila S, Roche F, et al. Von willebrand factor links primary hemostasis to innate immunity. *Nat Commun* 2022; 13: 6320.
56. Bryckaert M, Rosa JP, Denis CV, et al. Of von willebrand factor and platelets. *Cell Mol Life Sci* 2015; 72: 307–326.
57. Massberg S, Enders G, Melo Matos CD, et al. Fibrinogen deposition at the postschemic vessel wall promotes platelet adhesion during ischemia-reperfusion in vivo. *Blood* 1999; 94: 3829–3838.
58. Lindsberg PJ, Carpén O, Paetau A, et al. Endothelial ICAM-1 expression associated with inflammatory cell response in human ischemic stroke. *Circulation* 1996; 94: 939–945.
59. Bombeli T, Schwartz BR and Harlan JM. Adhesion of activated platelets to endothelial cells: evidence for a GPIIb/IIIa-dependent bridging mechanism and novel roles for endothelial intercellular adhesion molecule 1 (ICAM-1), $\alpha v\beta 3$ integrin, and GPIIb. *J Exp Med* 1998; 187: 329–339.
60. Tailor A, Cooper D and Granger DN. Platelet–vessel wall interactions in the microcirculation. *Microcirculation* 2005; 12: 275–285.
61. Gould DB, Phalan FC, Breedveld GJ, et al. Mutations in Col4a1 cause perinatal cerebral hemorrhage and porencephaly. *Science* 2005; 308: 1167–1171.
62. Gui T, Reheman A, Ni H, et al. Abnormal hemostasis in a knock-in mouse carrying a variant of factor IX with

- impaired binding to collagen type IV. *J Thromb Haemost* 2009; 7: 1843–1851.
63. Bridges JM, Dalby AM, Millar JH, et al. An effect of D-glucose on platelet stickiness. *Lancet* 1965; 1: 75–77.
 64. Giles JA, Greenhalgh AD, Denes A, et al. Neutrophil infiltration to the brain is platelet-dependent, and is reversed by blockade of platelet GPIIb/IIIa. *Immunology* 2018; 154: 322–328.
 65. Guzik TJ, West NE, Pillai R, et al. Nitric oxide modulates superoxide release and peroxynitrite formation in human blood vessels. *Hypertension* 2002; 39: 1088–1094.
 66. Zhao Y, Zhang J, Zhang J, et al. Diabetes mellitus is associated with shortened activated partial thromboplastin time and increased fibrinogen values. *Plos One* 2011; 6: e16470.
 67. Mafra D, Borges NA, Lindholm B, et al. Food as medicine: targeting the uraemic phenotype in chronic kidney disease. *Nat Rev Nephrol* 2021; 17: 153–171.